Results in Applied Mathematics 8 (2020) 100089

Contents lists available at ScienceDirect

Results in Applied Mathematics

journal homepage: www.elsevier.com/locate/results-in-applied-mathematics

A high order hybridizable discontinuous Galerkin method for incompressible miscible displacement in heterogeneous media

Maurice S. Fabien [a,1], Matthew Knepley [b], Beatrice Riviere [c,*,2]

[a] Division of Applied Mathematics, Brown University, Providence, RI, United States of America
[b] Department of Computer Science and Engineering, State University of New York at Buffalo, Buffalo, NY, United States of America
[c] Department of Computational and Applied Mathematics, Rice University, Houston, TX, United States of America

ARTICLE INFO

Article history:
Received 23 August 2019
Received in revised form 10 December 2019
Accepted 17 December 2019
Available online 15 January 2020

Keywords:
High order
Discontinuous Galerkin
Hybridization
Porous media
Quarter five spot
Heterogeneity

ABSTRACT

An hybridizable discontinuous Galerkin method of arbitrary high order is formulated to solve the miscible displacement problem in porous media. The spatial discretization is combined with a sequential algorithm that decouples the flow and the transport equations. Hybridization produces a linear system for the globally coupled degrees of freedom, that is smaller in size compared to the system resulting from the interior penalty discontinuous Galerkin methods. We study the impact of increasing the polynomial order on the accuracy of the solution. Numerical experiments show that the method converges optimally and that it is robust for highly heterogeneous porous media in two and three dimensions.

1. Introduction

Miscible displacement in porous media is a fundamental process for modeling groundwater flows and enhanced oil recovery [1–7]. The velocity of the fluid mixture satisfies Darcy's law with a viscosity that varies in time because it depends on the solvent concentration. The transport equation models the propagation of the solvent through the medium and is coupled with the flow equations via diffusive and advective fluxes. The overall mathematical model is a system of coupled nonlinear partial differential equations. There is a vast literature on first order methods used to solve the miscible displacement problems and several discretizations have been proposed. The works [8–10] use a finite element method whereas the work [11] combines the finite element method and the method of characteristics. Recently there has been a strong interest in developing high order methods with polynomial approximation of degree greater than or equal to three. High order methods have been shown to be computationally efficient on coarse meshes.

The class of discontinuous Galerkin (DG) methods easily handles high order approximations because of the lack of continuity constraints between the mesh elements. The works [12–15] introduce interior penalty discontinuous Galerkin methods for the miscible displacement problem and approximate the fluid pressure and the solvent concentration by discontinuous piecewise polynomials of degree up to four. The authors demonstrate the robustness of the DG methods

* Corresponding author.
E-mail addresses: fabien@brown.edu (M.S. Fabien), knepley@buffalo.edu (M. Knepley), riviere@rice.edu (B. Riviere).

[1] Research conducted at Department of Computational and Applied Mathematices, Rice University.

[2] Supported in part by NSM-DMS.

https://doi.org/10.1016/j.rinam.2019.100089

for heterogeneous media and for viscous fingering. The papers also show the accuracy in the concentration front when quadratic or cubic polynomials are used, as opposed to linears.

The novel contribution of this work is to formulate and apply an hybridizable discontinuous Galerkin (HDG) method of high order for solving the miscible displacement problem in heterogeneous media. Hybridization has been shown to significantly reduce the total number of globally coupled degrees of freedom for a variety of model problems [16–18], as well as the number of nonzero entries in the discretization matrix [19,20]. The reduction in degrees of freedom (and total non zero entries in discretization operators) is of great importance, as we use high order accurate approximations for the simulation of complex flow and transport systems. This paper approximates the unknowns by polynomials with degree up to sixteen and it contains several numerical simulations in two and three dimensional porous media with varying permeability fields. The HDG method employs numerical fluxes (equivalent to Lagrange multipliers) as trace unknowns that are defined on the mesh skeleton. Once the trace unknowns are solved for, they become boundary data of small local problems for the element unknowns. Hybridization of the DG method has two important consequences: first, the global matrix is of reduced size compared to standard DG; and second, the uniqueness of the trace unknowns on the mesh skeleton stabilizes the discontinuous approximation of the flow and transport in highly heterogeneous media, so that the amount of overshoot and undershoot is minimal and does not increase with time. In our work, we do not post-process the concentration with a slope limiting technique. An approach related to the HDG scheme called the hybrid high order method [21], was applied to the miscible displacement problem in [22] on a variety of meshes in two dimensions. The method employs local gradient reconstruction operators (also known as lift operators) in space and a Crank–Nicolson time stepping. Up to degree three polynomials are considered, and it is demonstrated that a piecewise linear basis provides the best balance between computational efficiency and accuracy. The novelty of our work compared to [22] consists of several aspects: we do not use local gradient reconstruction, we use a first order in time and the numerical examples employ polynomial degrees up to 16.

The HDG method enjoys several properties: it has optimal order of convergence $k+1$ in the L^2 norm for all approximate variables if polynomials of degree k are employed; it possesses a local postprocessing that can enhance the accuracy of the scalar variable (with an order of accuracy $k+2$); and it retains favorable aspects of classical DG methods (e.g. local mass conservation, ability to handle unstructured meshes, etc.). The HDG method for coupled flow and transport satisfies a compatibility property defined in [23]. Furthermore, if more accuracy is desired, one can resort to a simple element by element postprocessing that projects the flow velocity into an $H(\text{div}, \Omega)$-conforming subspace. This postprocessing is available since the scalar and flux unknowns converge optimally and the normal component of the numerical flux for the HDG method is single valued [16]. HDG methods for the convection–diffusion problem have been studied by numerous authors, including the case of convection-dominated diffusion, and small diffusion coefficients [16,24–27]. To the best of our knowledge, there are very few papers on HDG for complex porous media flows. Recently, we developed an HDG method for solving immiscible two-phase flows in porous media [28], which is a different application than miscible displacement. In two-phase flows, capillary pressure (difference between phase pressures) plays an important role, whereas miscible displacement is a single phase flow and the diffusion–dispersion matrix plays a critical role. Finally, we point out that hybridization has been applied to classical mixed finite element methods [29,30], which alleviates the difficulty in solving saddle-point systems arising from mixed finite element methods. A recent work combines the hybrid mixed finite element method for solving the flow equations and the classical discontinuous Galerkin method for solving the transport equation for the miscible displacement problem [31].

A brief outline of the paper is now given. Section 2 contains the model problem and Section 3 the numerical scheme. Simulations are shown in Section 4. Conclusions follow.

2. Model problem

The displacement of one incompressible fluid by another in the domain $\Omega \subset \mathbb{R}^d$ (for $d = 2, 3$) over the time interval $(0, T)$ is governed by the following coupled equations:

$$\nabla \cdot \boldsymbol{u} = s^I - s^P, \quad \boldsymbol{u} = -\frac{K}{\mu(c)} \nabla p, \qquad \text{in } \Omega \times (0, T], \tag{1}$$

$$\phi \frac{\partial c}{\partial t} + \nabla \cdot (\boldsymbol{u} c + \boldsymbol{q}) = s^I \bar{c} - s^P c, \quad \boldsymbol{q} = -\boldsymbol{D}(\boldsymbol{u}) \nabla c, \qquad \text{in } \Omega \times (0, T]. \tag{2}$$

The primary unknowns are the pressure of the fluid mixture denoted by p, the concentration of the solvent in the fluid mixture denoted by c, the fluid mixture velocity denoted by $\boldsymbol{u}$ and the diffusive flux $\boldsymbol{q}$. The coefficient μ is the viscosity of the fluid mixture and ϕ and K are respectively the porosity and permeability of the porous medium. The porosity is a positive constant and the permeability is a piecewise constant field with values bounded below by a positive constant. The functions s^I and s^P are the flow rates at injection and production wells respectively, and $\bar{c}$ is the solvent concentration prescribed at the injection wells. In the definition of the diffusive flux, $\boldsymbol{q}$, the dispersion–diffusion matrix, $\boldsymbol{D}(\boldsymbol{u})$, depends nonlinearly on the velocity [32]:

$$\boldsymbol{D}(\boldsymbol{u}) = (d_m + \alpha_t \|\boldsymbol{u}\|) \boldsymbol{I} + (\alpha_\ell - \alpha_t) \frac{\boldsymbol{u}\boldsymbol{u}^T}{\|\boldsymbol{u}\|},$$

where d_m is the molecular diffusion, α_t and α_ℓ are the tangential and longitudinal dispersivities, respectively, $\boldsymbol{I}$ is the identity matrix and $\|\cdot\|$ denotes the Euclidean norm. The values $d_m, \alpha_t, \alpha_\ell$ are positive constants. The viscosity of the fluid mixture is a continuous function and it satisfies the common quarter-power mixing law [33]

$$\mu(c) = (c(\mu_s)^{-0.25} + (1-c)(\mu_o)^{-0.25})^{-4},$$

where μ_s and μ_o are the viscosity of the solvent and resident fluid respectively.

Let $\boldsymbol{n}$ denote the outward unit normal vector to Ω. The system is completed by no flow boundary conditions and an initial condition for the concentration:

$$\begin{aligned} \boldsymbol{u}\cdot\boldsymbol{n} &= 0, && \text{on } \partial\Omega\times(0,T],\\ \boldsymbol{D}(\boldsymbol{u})\nabla c\cdot\boldsymbol{n} &= 0, && \text{on } \partial\Omega\times(0,T],\\ c(\cdot,t) &= c^0, && \text{in } \Omega\times\{0\}. \end{aligned}$$

3. Discretization

The domain Ω is partitioned into a mesh, $\mathcal{E}_h$, made of quadrilaterals in two dimensions and hexahedra in three dimensions. The skeleton of the mesh is denoted by Γ_h and it is the set of all edges in two dimensions or faces in three dimensions. The set of interior edges/faces is denoted by Γ_h^i and the set of boundary edges/faces by Γ_h^∂. The collection of all element boundaries is denoted by $\partial\mathcal{E}_h$, and it is distinct from Γ_h, as interior edges (or faces) are duplicated. For each mesh element E (resp. face e), let $\mathbb{Q}_k(E)$ (resp. $\mathbb{Q}_k(e)$), denote the set of polynomials over E (resp. e), of degree k in each coordinate direction. Throughout the paper, we denote by $\boldsymbol{n}_E$ the unit normal vector outward of a mesh element E. For each interior face, e, shared by two elements, say E_i and E_j with $i<j$, we uniquely define the normal vector $\boldsymbol{n}_e$ pointing outward of E_i. With this choice of direction for the normal vector, the jump $[w]$ and average $\{w\}$ of scalar function w are uniquely defined by:

$$[w] = w|_{E_i} - w|_{E_j}, \quad \{w\} = \frac{1}{2}(w|_{E_i} + w|_{E_j}).$$

The discrete spaces are

$$\begin{aligned} W_h &= \{w\in L^2(\Omega) : w|_E \in \mathbb{Q}_k(E), \quad \forall E\in\mathcal{E}_h\},\\ \boldsymbol{V}_h &= (W_h)^d,\\ M_h &= \{\zeta\in L^2(\Gamma_h) : \zeta|_e \in \mathbb{Q}_k(e), \quad \forall e\in\Gamma_h\}. \end{aligned} \tag{3}$$

3.1. Semi-discrete scheme

Eqs. (1)–(2) are discretized by the hybridizable discontinuous Galerkin method. We employ the usual notation $(\cdot,\cdot)_{\mathcal{O}}$ for the L^2 inner-product over an open domain $\mathcal{O}$. The semi-discrete scheme is: find $\boldsymbol{u}_h, \boldsymbol{q}_h$ in $\boldsymbol{V}_h$, p_h, c_h in W_h, $\widehat{p}_h, \widehat{c}_h$ in M_h such that for all $(\boldsymbol{v}, w, \zeta)$ in $\boldsymbol{V}_h\times W_h\times M_h$

$$(\mu(c_h)K^{-1}\boldsymbol{u}_h, \boldsymbol{v})_E - (p_h, \nabla\cdot\boldsymbol{v})_E + (\widehat{p}_h, \boldsymbol{v}\cdot\mathbf{n}_E)_{\partial E} = 0, \tag{4}$$

$$-(\boldsymbol{u}_h, \nabla w)_E + (\boldsymbol{u}_h\cdot\boldsymbol{n}_E + p_h - \widehat{p}_h, w)_{\partial E} = (s^I - s^P, w)_E, \tag{5}$$

$$(\boldsymbol{D}(\boldsymbol{u}_h)^{-1}\boldsymbol{q}_h, \boldsymbol{v})_E - (c_h, \nabla\cdot\boldsymbol{v})_E + (\widehat{c}_h, \boldsymbol{v}\cdot\boldsymbol{n}_E)_{\partial E} = 0, \tag{6}$$

$$\begin{aligned} &(\phi\frac{\partial c_h}{\partial t}, w)_E - (\boldsymbol{u}_h c_h + \boldsymbol{q}_h, \nabla w)_E\\ &\quad + (\boldsymbol{q}_h\cdot\boldsymbol{n}_E + \tau(c_h - \widehat{c}_h) + \widehat{c}_h\boldsymbol{u}_h\cdot\boldsymbol{n}_E, w)_{\partial E} = (s^I\bar{c} - s^P c_h, w)_E, \end{aligned} \tag{7}$$

for all E in $\mathcal{E}_h$, and

$$(\widehat{p}_h, \zeta)_e = (\{p_h\} + \frac{1}{2}[\boldsymbol{u}_h\cdot\boldsymbol{n}_e], \zeta)_e, \tag{8}$$

$$(\widehat{c}_h(\{\tau\} - \frac{1}{2}[\boldsymbol{u}_h\cdot\boldsymbol{n}_e]), \zeta)_e = (\frac{1}{2}[\boldsymbol{q}_h\cdot\boldsymbol{n}_e] + \{\tau c_h\}, \zeta)_e, \tag{9}$$

for all e in Γ_h^i, and

$$(\widehat{p}_h, \zeta)_e = (p_h, \zeta)_e, \tag{10}$$

$$(\widehat{c}_h(\tau - \frac{1}{2}\boldsymbol{u}_h\cdot\boldsymbol{n}_e), \zeta)_e = (\frac{1}{2}\boldsymbol{q}_h\cdot\boldsymbol{n}_e + \tau c_h, \zeta)_e, \tag{11}$$

for all e in Γ_h^∂.

The coefficient τ is a stabilization parameter that may take a different value on each mesh element [16]. From [25,34], we set

$$\tau(\boldsymbol{x}) = |\boldsymbol{u}_h(\boldsymbol{x}) \cdot \boldsymbol{n}_E| + \max(\|\boldsymbol{D}(\boldsymbol{u}_h(\boldsymbol{x}))\|_\infty, 1), \forall \boldsymbol{x} \in \partial E, \quad \forall E \in \mathcal{E}_h.$$

3.2. Fully discrete scheme

It is well known that the pressure and velocity fields evolve in time much more slowly than the concentration. Therefore the sequential algorithm, that decouples the pressure and velocity equations from the concentration and diffusive flux equations, is widely accepted in the literature. Let Δt denote the time step. For the initial condition, we define $c_h^0 \in W_h$ satisfying

$$(c_h^0, w)_E = (c^0, w)_E, \quad \forall E \in \mathcal{E}_h, \quad \forall w \in W_h.$$

The fully discrete scheme is given in two steps. First, given c_h^{n-1} in W_h, find $\boldsymbol{u}_h^n$ in $\boldsymbol{V}_h$, p_h^n in W_h and $\widehat{p}_h^n$ in M_h such that

$$(\mu(c_h^{n-1})K^{-1}\boldsymbol{u}_h^n, \boldsymbol{v})_E - (p_h^n, \nabla \cdot \boldsymbol{v})_E + (\widehat{p}_h^n, \boldsymbol{v} \cdot \mathbf{n}_E)_{\partial E} = 0, \quad \forall E \in \mathcal{E}_h, \tag{12}$$

$$-(\boldsymbol{u}_h^n, \nabla w)_E + (\boldsymbol{u}_h^n \cdot \boldsymbol{n}_E + p_h^n - \widehat{p}_h^n, w)_{\partial E} = (s^I - s^P, w)_E, \quad \forall E \in \mathcal{E}_h, \tag{13}$$

$$(\widehat{p}_h^n, \zeta)_e = (\{p_h^n\} + \frac{1}{2}[\boldsymbol{u}_h^n \cdot \boldsymbol{n}_e], \zeta)_e, \quad \forall e \in \Gamma_h^i, \tag{14}$$

$$(\widehat{p}_h^n, \zeta)_e = (p_h^n + \frac{1}{2}\boldsymbol{u}_h^n \cdot \boldsymbol{n}_e, \zeta)_e, \quad \forall e \in \Gamma_h^\partial, \tag{15}$$

for all $(\boldsymbol{v}.w, \zeta)$ in $\boldsymbol{V}_h \times W_h \times M_h$.

Second, find $\boldsymbol{q}_h^n$ in $\boldsymbol{V}_h$, c_h^n in W_h and $\widehat{c}_h^n$ in M_h such that

$$(\boldsymbol{D}(\boldsymbol{u}_h{}^n)^{-1}\boldsymbol{q}_h^n, \boldsymbol{v})_E - (c_h^n, \nabla \cdot \boldsymbol{v})_E + (\widehat{c}_h^n, \boldsymbol{v} \cdot \boldsymbol{n}_E)_{\partial E} = 0, \quad \forall E \in \mathcal{E}_h, \tag{16}$$

$$(\phi \frac{c_h^n - c_h^{n-1}}{\Delta t}, w)_E - (\boldsymbol{u}_h^n c_h + \boldsymbol{q}_h^n, \nabla w)_E + (\boldsymbol{q}_h^n \cdot \boldsymbol{n}_E, w)_{\partial E}$$
$$+ (\tau(c_h^n - \widehat{c}_h^n) + \widehat{c}_h^n \boldsymbol{u}_h^n \cdot \boldsymbol{n}_E, w)_{\partial E} = (s^I \bar{c} - s^P c_h^n, w)_E, \quad \forall E \in \mathcal{E}_h, \tag{17}$$

$$(\widehat{c}_h^n(\tau - \frac{1}{2}[\boldsymbol{u}_h^n \cdot \boldsymbol{n}_e]), \zeta)_e = (\frac{1}{2}[\boldsymbol{q}_h^n \cdot \boldsymbol{n}_e] + \tau\{c_h^n\}, \zeta)_e, \quad \forall e \in \Gamma_h^i, \tag{18}$$

$$(\widehat{c}_h^n(\tau - \frac{1}{2}\boldsymbol{u}_h^n \cdot \boldsymbol{n}_e), \zeta)_e = (\frac{1}{2}\boldsymbol{q}_h^n \cdot \boldsymbol{n}_e + \tau c_h^n, \zeta)_e, \quad \forall e \in \Gamma_h^\partial, \tag{19}$$

for all $(\boldsymbol{v}.w, \zeta)$ in $\boldsymbol{V}_h \times W_h \times M_h$.

3.3. Local and global solves

The main advantage of HDG methods is that the hybridization decouples the solution of the unknowns $p_h^n, \boldsymbol{u}_h^n, c_h^n, \boldsymbol{q}_h^n$ from the solution of the trace unknowns $\widehat{p}_h^n$ and $\widehat{c}_h^n$. The solution of the trace unknowns requires solving a global system whereas the solution of the other unknowns is done locally on each mesh element, which is embarrassingly parallel. Since the trace unknowns live on the mesh skeleton, the size of the global system is smaller compared to the size of the global system in a standard DG method. Specific information regarding total degrees of freedom and total nonzero entries in the discretization matrix for different element types can be found in [19,20,35]. For clarity we consider some quantitative examples to illustrate this point.

3.3.1. Two-dimensional quadrilateral mesh

In this section we compare the degrees of freedom for a classical DG and HDG scheme applied to problems (1) and (2). We consider a uniform mesh of the unit square with $N \times N$ quadrilateral elements. The number of degrees of freedom of the global system for HDG is proportional to the number of edges and is equal to $4(k+1)(N^2+N)$. The number of degrees of freedom for the global system for the classical DG methods is proportional to the number of elements and is equal to $2((k+1)^2N^2)$. This yields a ratio R that is smaller than one whenever k is greater than $1 + 2N^{-1}$.

$$R = \frac{\text{HDG}_{\text{coupled DOFs}}}{\text{DG}_{\text{coupled DOFs}}} = \frac{2(N+1)}{(k+1)N}.$$

Fig. 1 visualizes this ratio, for various values of k and N. Fig. 1a shows that for a given polynomial degree, the ratio decreases. However, much more substantial reductions for R are obtained if the polynomial degree is increased, which is clear from Fig. 1b. For instance, for $k = 3$ and $N \geq 50$, the HDG method has about half the number of globally coupled degrees of freedom than classical DG.

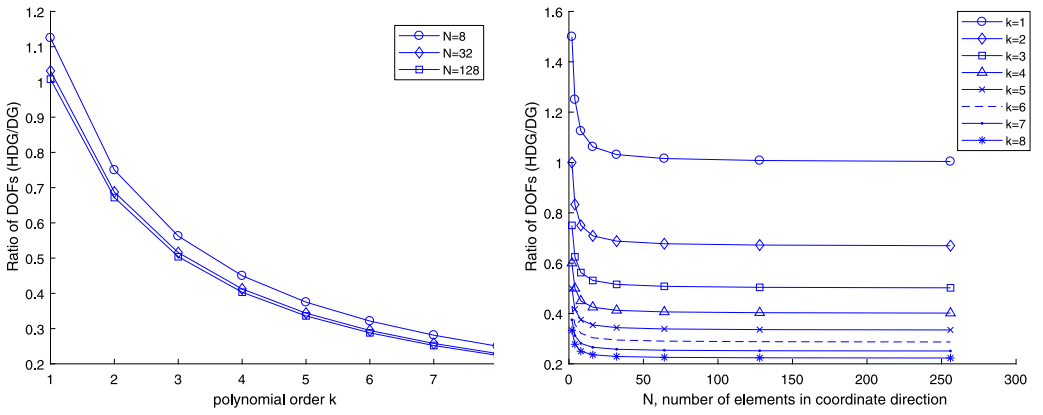

(a) Ratio vs k (b) Ratio vs N

Fig. 1. Ratio of globally coupled degrees of freedom for HDG to classical DG for quadrilateral meshes.

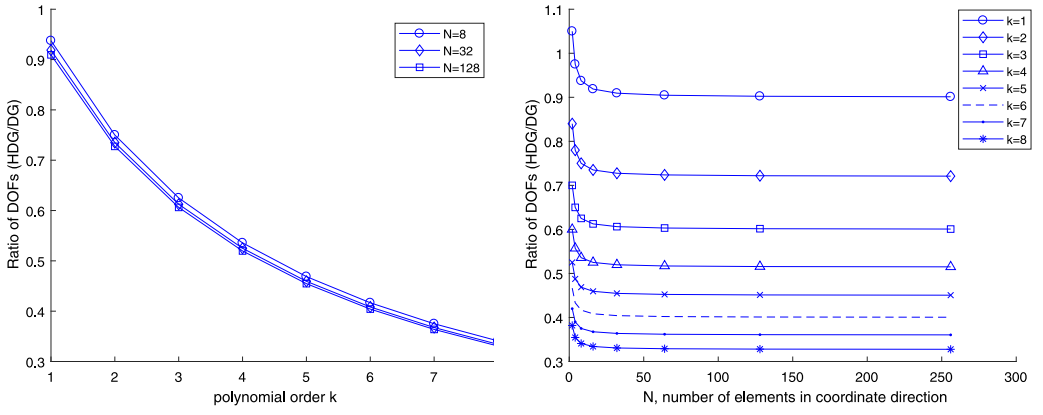

(a) Ratio vs k (b) Ratio vs N

Fig. 2. Ratio of globally coupled degrees of freedom for HDG to classical DG for tetrahedral meshes.

3.3.2. Three-dimensional tetrahedral mesh

We consider the unit cube partitioned into $N \times N \times N$ hexahedra. Each hexahedron is then divided into five tetrahedra. In this case, the number of degrees of freedom of the global system for HDG is equal to $(k+2)(k+1)(6N^3+2N^2)$ whereas the number of degrees of freedom for the global system for the classical DG methods is equal to $5(k+3)(k+2)(k+1)N^3/3$. The ratio R is then less than one whenever k is greater than $(3+6N^{-1})/5$. We plot in Fig. 2 the ratio for different values of k and N. Similar conclusions to the 2D case can be made.

3.3.3. Linear solvers

Since our algorithm decouples flow and transport, multiple linear systems are to be solved at every time step. In the most simple situation only two linear solves are needed per time step, one for obtaining the pressure and velocity and the other for concentration. In some situations one could lag the pressure/velocity update and use it for multiple time steps before obtaining a new update. Iterative coupling and high order time stepping may be utilized to enhance the solution, which increases the number of linear solves that are needed per time step. Efficient linear solvers are required for this class of problems, as the dominant cost occurs during this phase of the simulation.

3.4. Local solves

The local solves are performed locally on each mesh element, and give rise to a sequence of small dense matrix–matrix operations. As such, this process is efficiently parallelizable. In particular, we use highly optimized dense matrix linear

algebra subroutines [36,37]. Our previous work explains how to implement these local solves efficiently in a massively parallel environment [38].

3.5. Global solves

On the other hand, the globally coupled problem for the trace unknowns gives rise to a large sparse linear system which must be solved for at each time step. To do this, a multigrid technique is utilized. We begin the multigrid process with the so-called polynomial-multigrid scheme (or p-multigrid) [39–42], which defines a level hierarchy by polynomial degree. That is, the matrix associated with the fine level is the discretization with the largest polynomial degree used (k). The lower levels are defined by the discretization with smaller polynomial degrees, $k-1, k-2, \ldots, 1$. The resulting multigrid scheme is very effective, and we observe roughly 6 to 12 iterations per solve. Below we outline key features of the global solver.

In order to move between the levels, prolongation and restriction operators are required. These spaces are nested, as the mesh spacing is fixed, and only the polynomial degree is altered. This allows us to take advantage of straightforward prolongation and restriction operators, which are element local. The prolongation operator is the natural embedding from the space of polynomials of degree $k-1$ into the space of polynomials of degree k. To preserve symmetry, the restriction operator is taken as the transpose of the prolongation operator.

A key ingredient for multigrid is the relaxation or smoother operator. One challenge in designed or selecting a smoother is that high polynomial degrees ($k > 1$) as well as heterogeneous coefficients worsen the conditioning of the globally coupled discretization matrix. In order to overcome these challenges, a strong relaxation method is needed. In this paper we use a minimal overlapping additive Schwarz scheme [43]. This smoother performs well in the context of flow and transport applications.

Once the multigrid process reaches the coarse grid level (associated with polynomial degree $k = 1$ in our work), we solve the resulting system using the GAMG solver from PETSc [44–46]. If the mesh size is very small, one can continue the hierarchy using geometric multigrid [38,47]. However, in our work, we are able to use relatively coarse meshes due to the adoption of large polynomial degrees.

4. Numerical experiments

4.1. Manufactured solution in 2D

To test the convergence properties of our method, we use the method of manufactured solutions on the unit square partitioned into $N \times N$ quadrilateral elements. For simplicity, we use Dirichlet boundary conditions, which are obtained through the following prescribed solutions:

$$p(x, y, t) = 1 + xy \tanh(1-x)\tanh(1-y)\exp(-t),$$
$$c(x, y, t) = \cos(t)\sin(\pi x)\sin(\pi y)/(2\pi)^2.$$

The following values are chosen for this test:

$$K = 9.44 \cdot 10^{-3}, \phi = 0.2, d_m = 1, \alpha_\ell = 1.8 \cdot 10^{-5}, \alpha_t = 1.8 \cdot 10^{-6}.$$

The quarter power mixing law is used with viscosity ratio $\mu_o/\mu_s = 2$. We set $\Delta t = 0.1/((k+1)kN^2)$, and $T = 0.5$. We vary the mesh size and the polynomial degree. Table 1 shows the errors in the L^2 norm and convergence rates for the pressure, velocity, concentration and diffusive flux. The HDG scheme results in optimal rates of $k+1$ in the L^2 norm.

4.2. Quarter-five spot in homogeneous medium

In this example, the domain, $\Omega = [0, 1000]^2$, has an injection well at the bottom left corner and a production well at the right top corner. The wells are defined by the source/sink terms, which are piecewise constant with compact support. That is, s^I is nonzero on $[0, 100] \times [0, 100]$ and s^P is nonzero on $[900, 1000] \times [900, 1000]$. The constants are determined by the following constraint:

$$\int_\Omega s^I = \int_\Omega s^P = 0.28.$$

Viscosity is the same as in the previous example. The other physical parameters for this example are:

$$K = 10^{-10}, \phi = 0.2, d_m = 10^{-9}, \alpha_\ell = 1.8 \cdot 10^{-5}, \alpha_t = 1.8 \cdot 10^{-6}, \bar{c} = 1.$$

In this classical test problem, the solvent fluid is injected at the lower left corner, and displaces the fluid mixture to the upper right corner [48]. A uniform quadrilateral mesh of 1024 elements is used, with discontinuous piecewise quartic basis functions. The final simulation time is $T = 10$ days, and we provide snapshots at $t = 2.5$, $t = 5.0$, $t = 7.5$, and $t = 10$. Our splitting algorithm allows for large timesteps, and in this case we fix $\Delta t = 0.1$ days. The solvent concentration is displayed in Fig. 3.

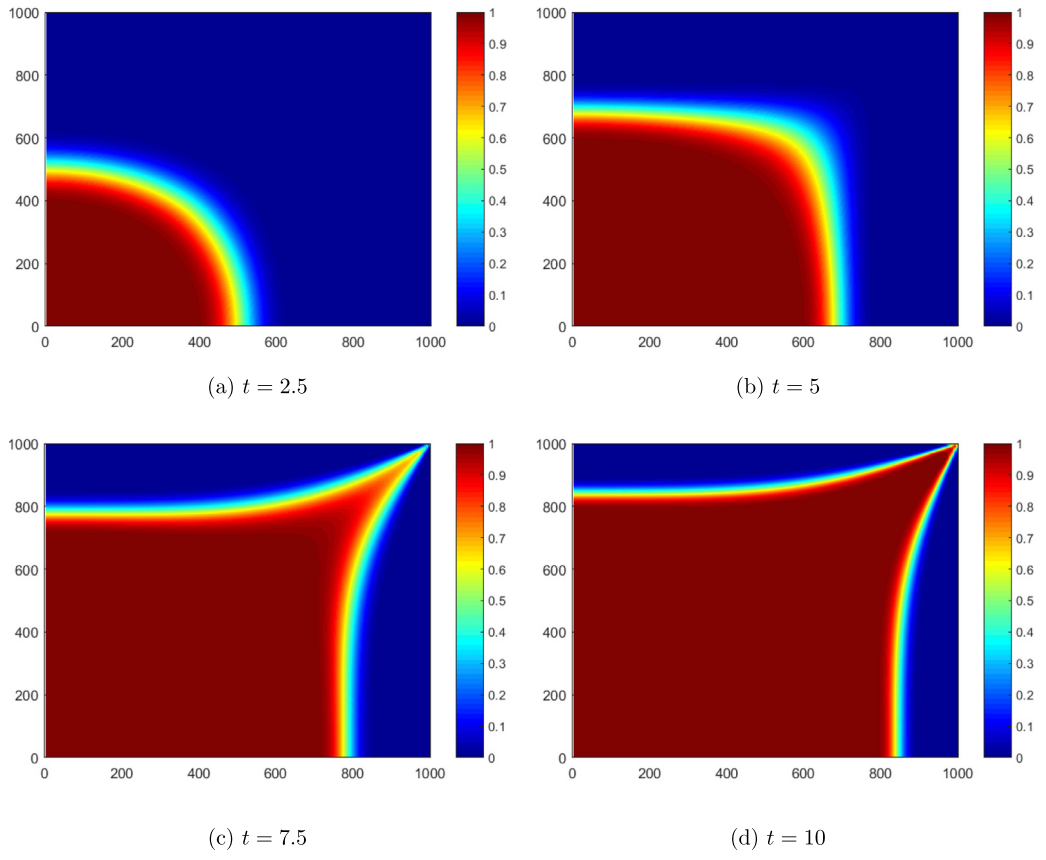

(a) $t = 2.5$ (b) $t = 5$

(c) $t = 7.5$ (d) $t = 10$

Fig. 3. Quarter-five spot problem in a homogeneous medium, with a mesh of 1024 elements, and polynomial order $k = 4$. Snapshots of the solvent profile are displayed at various times. The concentration travels from the injection well to the production well.

Table 1
Errors and convergence rates for $p_h, \boldsymbol{u}_h, c_h$, and $\boldsymbol{q}_h$, on a Cartesian mesh of $N \times N$ elements. The variables $\boldsymbol{u}_h, c_h, p_h$ and $\boldsymbol{q}_h$ converge at the rate of $k+1$ in the L^2 norm.

k	N	$\|p_h - p\|_{L^2(\Omega)}$		$\|\boldsymbol{u}_h - \boldsymbol{u}\|_{L^2(\Omega)}$		$\|c_h - c\|_{L^2(\Omega)}$		$\|\boldsymbol{q}_h - \boldsymbol{q}\|_{L^2(\Omega)}$	
		Error	Rate	Error	Rate	Error	Rate	Error	Rate
1	4	4.528e−03	–	9.965e−05	–	9.965e−04	–	4.538e−05	–
	8	1.364e−03	1.73	3.090e−05	1.68	3.090e−04	1.68	1.367e−05	1.73
	16	3.791e−04	1.84	8.674e−06	1.83	8.674e−05	1.83	3.799e−06	1.84
	32	1.002e−04	1.91	2.309e−06	1.90	2.309e−05	1.90	1.005e−06	1.91
	64	2.581e−05	1.95	5.969e−07	1.95	5.969e−06	1.95	2.587e−07	1.95
2	4	4.502e−05	–	1.032e−07	–	1.032e−05	–	4.502e−06	–
	8	6.466e−06	2.79	1.481e−08	2.80	1.481e−06	2.80	6.466e−07	2.79
	16	8.680e−07	2.89	1.997e−09	2.89	1.997e−07	2.89	8.680e−08	2.89
	32	1.125e−07	2.94	2.599e−10	2.94	2.599e−08	2.94	1.125e−08	2.94
3	4	3.517e−06	–	8.058e−09	–	8.058e−07	–	3.517e−07	–
	8	2.461e−07	3.83	5.650e−10	3.83	5.650e−08	3.83	2.461e−08	3.83
	16	1.624e−08	3.92	3.745e−11	3.91	3.745e−09	3.91	1.624e−09	3.92
	32	1.043e−09	3.96	2.413e−12	3.95	2.413e−10	3.95	1.043e−10	3.96
4	4	3.895e−06	–	1.203e−10	–	7.798e−07	–	3.895e−07	–
	8	1.333e−07	4.86	4.114e−12	4.87	3.092e−08	4.65	1.333e−08	4.86
	16	4.395e−09	4.92	1.366e−13	4.91	1.097e−09	4.81	4.395e−10	4.92
	32	1.413e−10	4.95	4.440e−15	4.94	3.666e−11	4.90	1.413e−11	4.95
5	4	1.476e−07	–	4.118e−11	–	4.914e−10	–	1.476e−08	–
	8	2.593e−09	5.83	7.192e−13	5.83	9.115e−12	5.75	2.593e−10	5.83
	16	4.303e−11	5.91	1.194e−14	5.91	1.573e−13	5.85	4.303e−12	5.91
	32	6.939e−13	5.95	1.935e−16	5.94	2.597e−15	5.92	6.939e−14	5.95

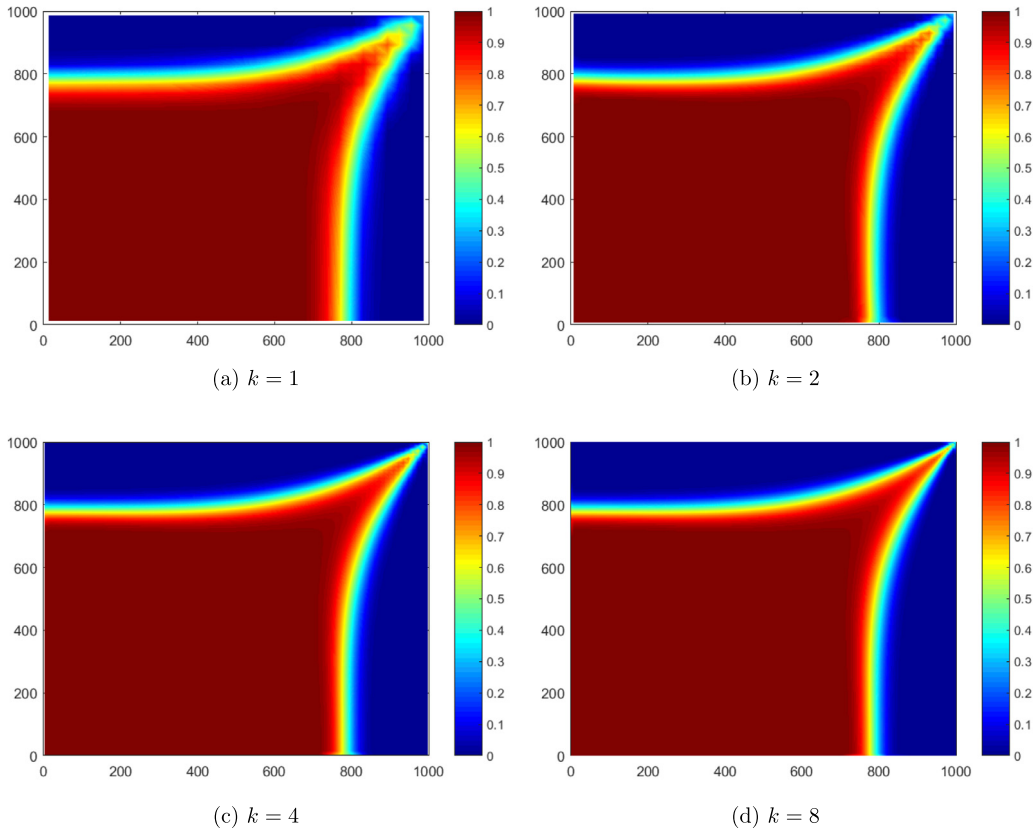

Fig. 4. Polynomial order study at $t = 7.5$, on a coarse mesh with 256 elements. As the polynomial order increases, the resolution of the concentration front is sharper.

Next, we study the effect of the polynomial order on the concentration profile. In Fig. 4, we show the concentration contours at $t = 7.5$ for several polynomial degrees ($k \in \{1, 2, 4, 8\}$) on a coarser mesh with 256 elements. Features near the concentration front (especially close to the production well) become more defined as the polynomial order is increased. To get a better sense for the convergence of the method, we examine the profile along the line $y = x$ at $t = 7.5$ for polynomial orders varying from piecewise linears to piecewise octics. Fig. 5 shows the full profile and three zoomed views. The full profile shows convergence of the method as the polynomial degree increases. The zoomed-views show that the concentration is sharper for higher polynomial degrees.

4.3. Quarter-five spot in medium with permeability lens

We now consider the miscible displacement problem in a porous medium where the permeability value is 10^{-10} everywhere except in the lens $[250, 500] \times [250, 500]$, where the value is 1000 times smaller. This region of lower permeability acts as an impermeable area for the fluid mixture. All other parameters are the same as in Section 4.2. The concentration contours at various times are depicted in Fig. 6, on a mesh with 1024 elements and with polynomial degree $k = 4$. As expected, the injected solvent avoids the region of lower permeability, while still traveling towards the production well. With high order approximations we are able to resolve the concentration front around the lens boundary with a fine resolution, as demonstrated by the sharpness of the front.

Fig. 7 shows the effect of increasing the polynomial order on the concentration solved on a coarser mesh of 256 elements. We fix $t = 7.5$, and increase the polynomial order in a geometric sequence ($k \in \{1, 2, 4, 8, 16\}$). The HDG method with all tested polynomial orders is able to capture the region of low permeability. Piecewise linears and quadratics give the most diffusive fronts particularly near the production well. Increasing the polynomial order has the impact of sharpening the concentration front and producing more accurate simulations on coarser meshes.

4.4. Quarter-five spot in two-dimensional highly heterogeneous media

In this section, we vary the permeability such that it is piecewise constant on each mesh element. The values of the permeability are chosen from three horizontal layers of the reservoir described in the SPE10 comparative solution

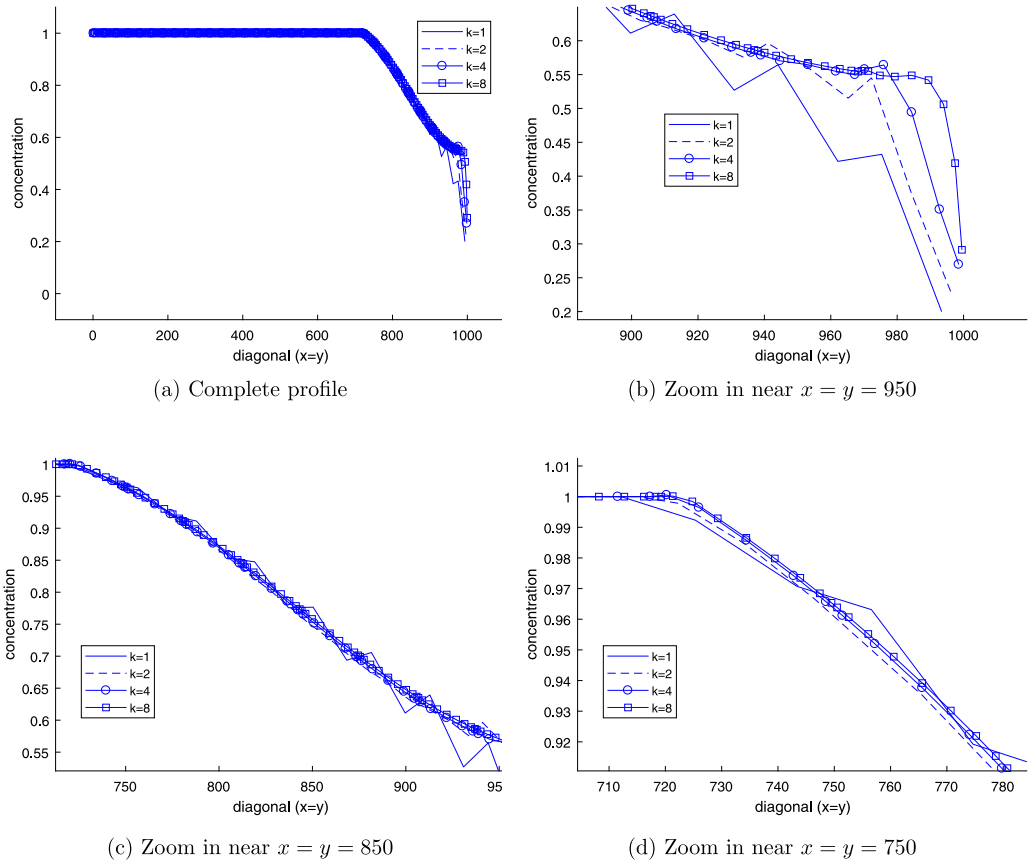

(a) Complete profile

(b) Zoom in near $x = y = 950$

(c) Zoom in near $x = y = 850$

(d) Zoom in near $x = y = 750$

Fig. 5. Concentration profile along the line $y = x$. Mesh contains 256 elements. Sharper concentration profiles are obtained with higher order polynomials.

project [49]. These permeability slices are scaled to a 64×64 grid, instead of the native 60×220 grid. Figs. 8a, 8b, and 8c show the selected permeability layers, which vary over the Talbert and Upper Ness formations. Layer 44 and 74 contain channels of higher permeability.

In all experiments we use a mesh with 4096 quadrilateral elements, and discontinuous piecewise quartic basis functions. All other parameters are the same as in Section 4.2. In Fig. 9, snapshots of the concentration are given at different times. The concentration profiles are displayed for each of the three permeability layers. Layer 1 corresponds to Figs. 9a, 9b, and 9c. Layer 44 corresponds to Figs. 9d, 9e, and 9f. Layer 74 corresponds to Figs. 9g, 9h, and 9i. The location of the channels in layer 44 is favorable to the flow direction from the bottom left corner to the top right corner of the domain. The other two layers contain impermeable regions that prevent the solvent to reach the production well at the same rate as for layer 44. This example shows the HDG method can handle highly heterogeneous porous media.

4.5. Three-dimensional domain with permeability lens

In this section we consider a porous medium with a permeability lens, analogous to the one described in Section 4.3 but in three dimensions. The domain is now $\Omega = [0, 1000]^3$. The permeability lens described in Section 4.3 is extruded in the z-direction, so that the region of lower permeability is a pillar. Production and injection wells are placed at opposite ends of the domain (e.g. near the origin and the coordinate (1000, 1000, 1000)). The remaining parameters are the same as in Section 4.3.

We use a structured mesh with 3072 tetrahedral elements, and piecewise quartic basis functions. Fig. 10 shows the Darcy velocity field, $\boldsymbol{u}_h$, The velocity is zero in the low permeability pillar and the fluid velocity is directed from the source to the sink (see Fig. 10)

Fig. 11 contains snapshots of the concentration at different times. The volumetric slices show that the fluid mixture avoids the region of lower permeability, as expected.

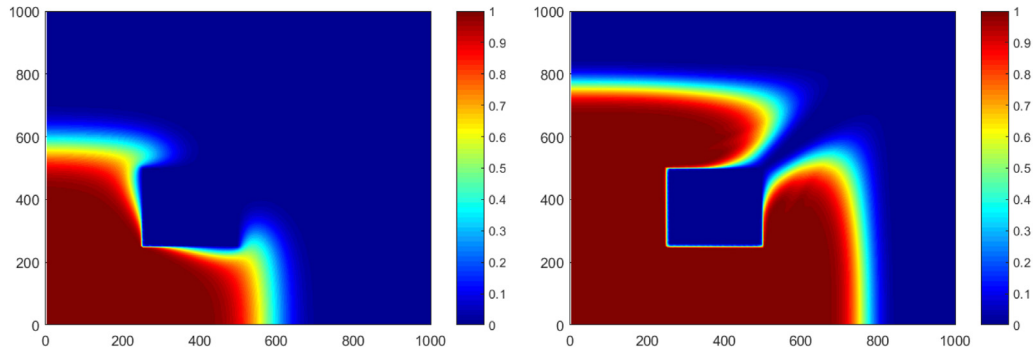

(a) $t = 2.5$ (b) $t = 5$

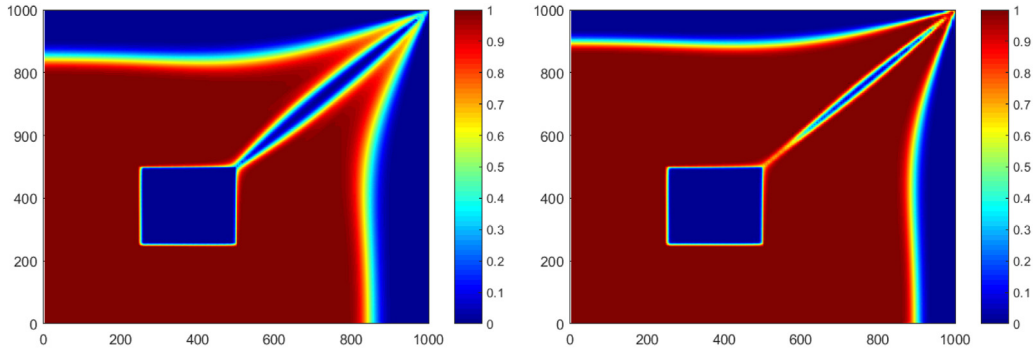

(c) $t = 7.5$ (d) $t = 10$

Fig. 6. Evolution of concentration for the permeability lens problem. The HDG method exhibits the correct behavior, since the concentration avoids the region of low permeability. Mesh with 1024 elements, and polynomial order $k = 4$.

4.6. Three-dimensional domain with heterogeneous permeability

In this example, the permeability field is highly heterogeneous and it is shown in Fig. 12. The values of the permeability are extracted from a $32 \times 64 \times 16$ region of the SPE10 comparative solution project [49]. The domain is $\Omega = [0, 50] \times [0, 100] \times [0, 25]$.

A quarter-five spot problem is set up as follows: we place an injection well at the coordinate $(0, 0, 25)$ and a production well at $(50, 100, 25)$, with $\int_\Omega s^I = \int_\Omega s^P = 1.5$. The mesh contains 174 080 tetrahedral elements, and we use piecewise cubic basis functions. All other parameters are the same as in Section 4.2. The concentration contours are displayed at various times in Figs. 13a, 13b, and 13c. The solvent propagates through the medium as expected, from the injection well to the production well.

5. Conclusion

This work presents a sequential hybridizable discontinuous Galerkin method for solving the miscible displacement problem in two and three dimensions. We show optimal convergence rates for manufactured solutions. We vary the polynomial degree and we demonstrate the accuracy of high polynomial approximation with respect to the sharpness of the concentration front. The method can easily handle heterogeneities in the permeability field, as shown in several examples of quarter-five spot problems.

Declaration of competing interest

The authors declare that they have no known competing financial interests or personal relationships that could have appeared to influence the work reported in this paper.

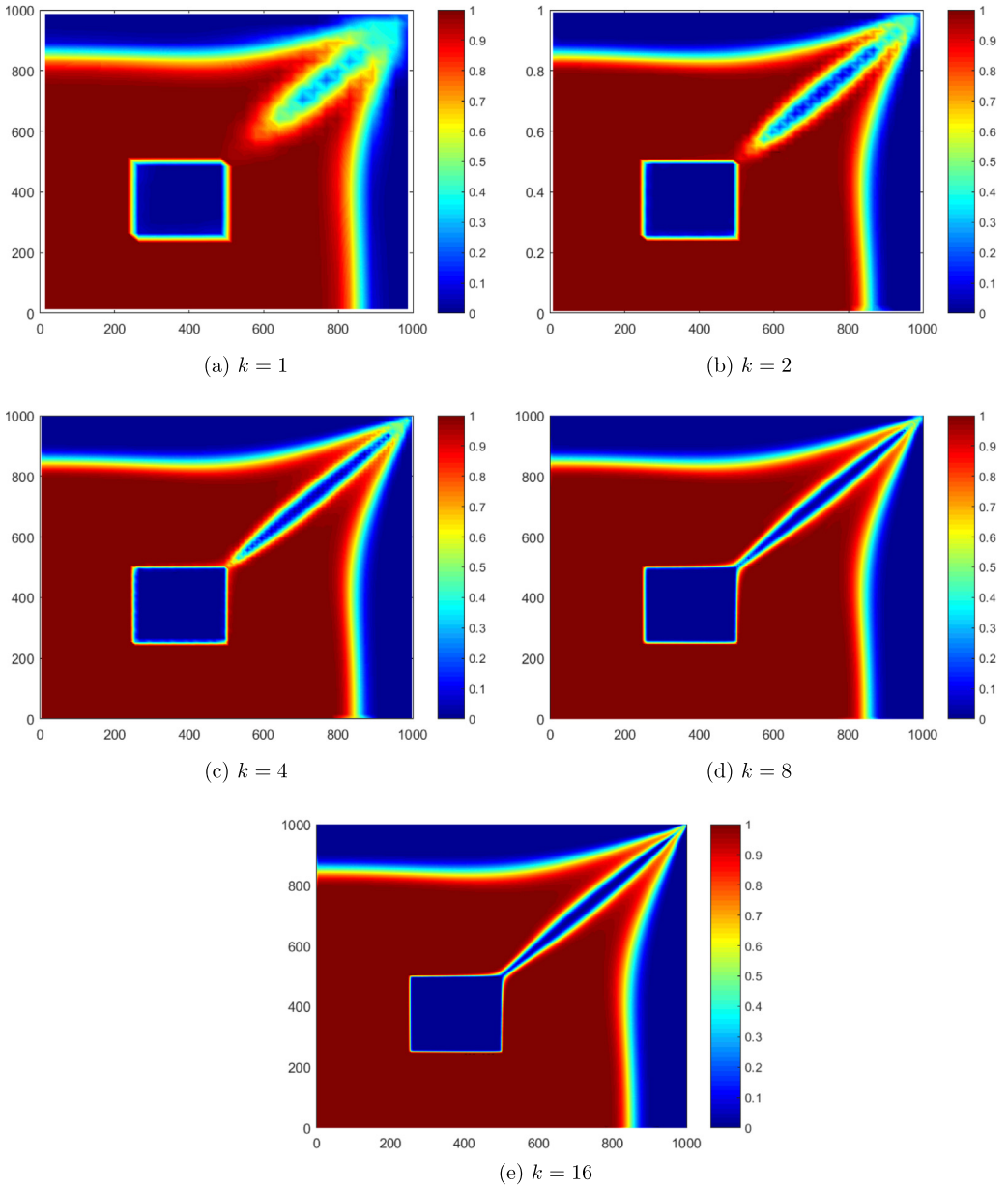

(a) $k = 1$ (b) $k = 2$

(c) $k = 4$ (d) $k = 8$

(e) $k = 16$

Fig. 7. Polynomial order study at $t = 7.5$, on a fixed mesh with 256 elements. As the polynomial degree increases, the approximation quality improves significantly.

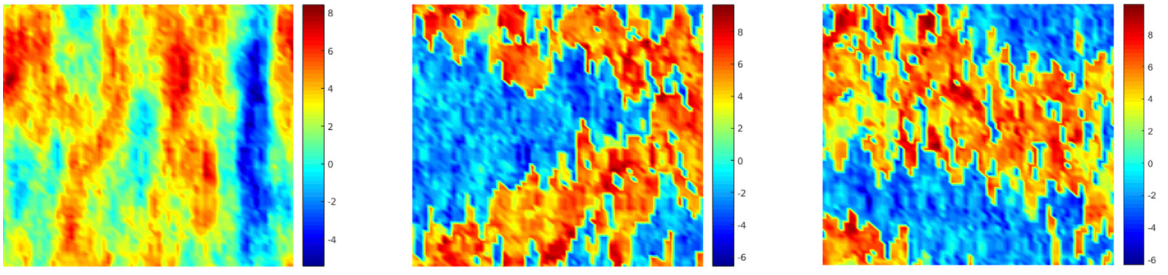

(a) Layer 1 (b) Layer 44 (c) Layer 74

Fig. 8. Permeability fields in log scale on 64 × 64 grid.

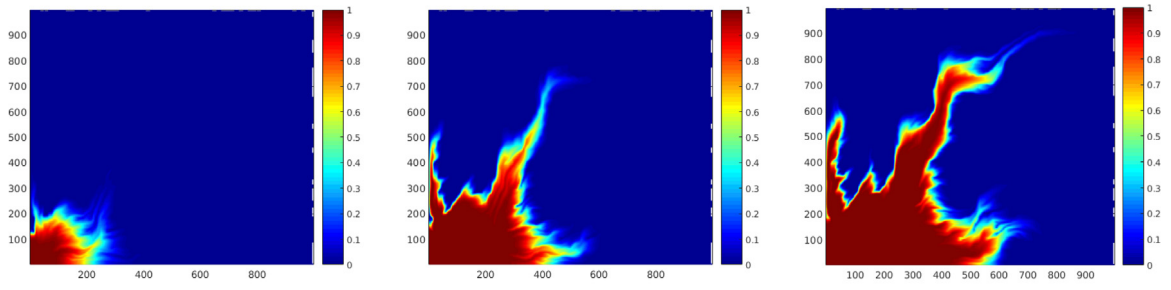

(a) Layer 1 at $t = 0.5$ days (b) Layer 1 at $t = 1.5$ days (c) Layer 1 at $t = 2.5$ days

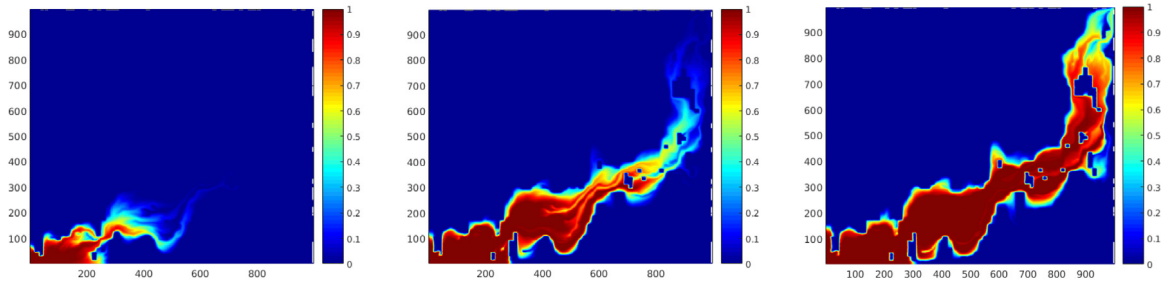

(d) Layer 44 at $t = 0.5$ days (e) Layer 44 at $t = 1.5$ days (f) Layer 44 at $t = 2.5$ days

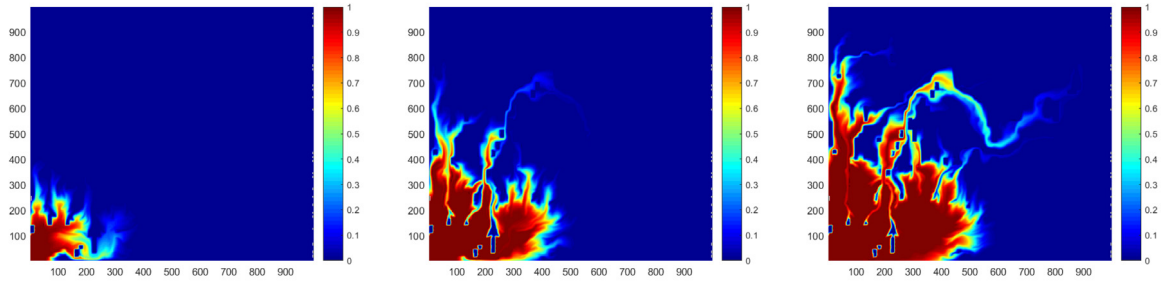

(g) Layer 74 at $t = 0.5$ days (h) Layer 74 at $t = 1.5$ days (i) Layer 74 at $t = 2.5$ days

Fig. 9. Concentration contours for quarter-five spot problem in two-dimensional heterogeneous media, with 4096 quadrilateral elements and discontinuous piecewise quartic polynomials.

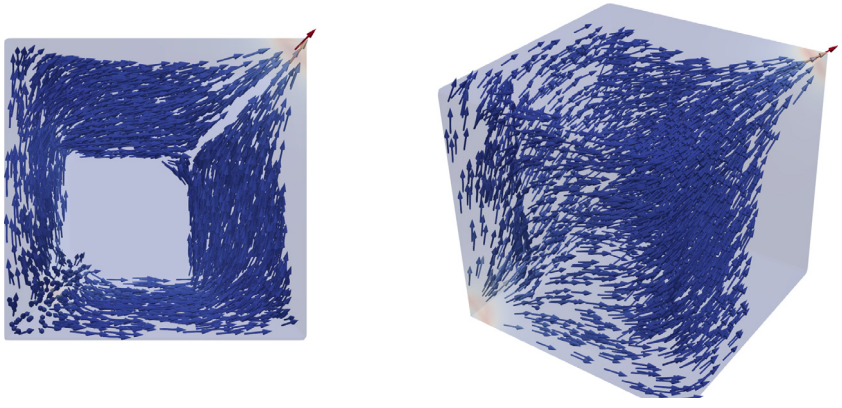

(a) Top-down view (b) Side view

Fig. 10. Miscible displacement in three dimensional domain. Darcy velocity field at $t = 7.5$ days (arrows not to scale), obtained with mesh with 3072 tetrahedral elements and with piecewise quartic basis functions.

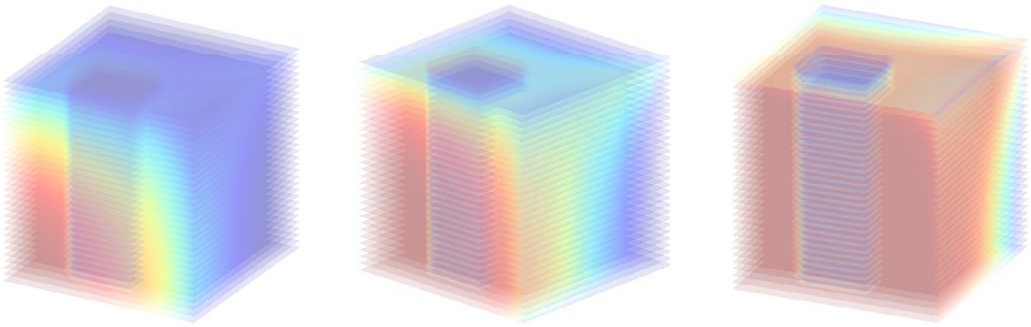

(a) $t = 2.5$ days (b) $t = 5$ days (c) $t = 7.5$ days

Fig. 11. Miscible displacement in three dimensional domain. Concentration snapshots at various times. The concentration is visualized as volume slices.

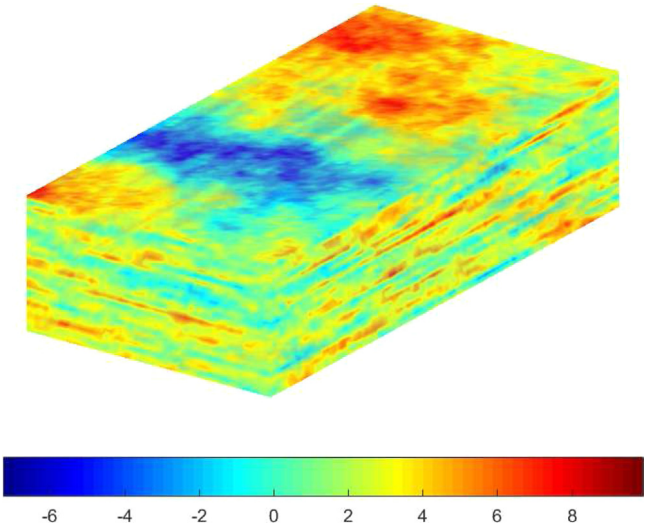

Fig. 12. Permeability field (log scale).

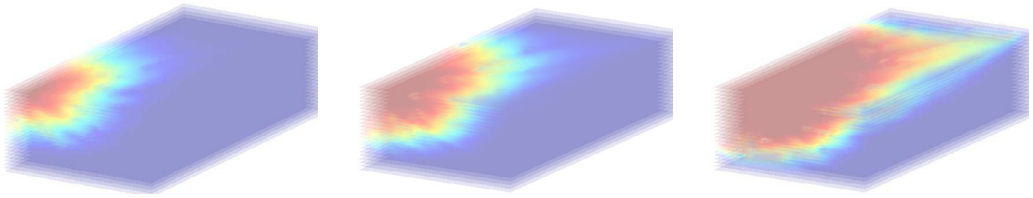

(a) $t = 1$ days (b) $t = 5$ days (c) $t = 8$ days

Fig. 13. Miscible displacement in heterogeneous medium. The concentration snapshots are visualized as volume slices.

CRediT authorship contribution statement

Maurice S. Fabien: Conceptualization, Methodology, Software, Writing - original draft, Writing - review & editing. **Matthew Knepley:** Conceptualization, Methodology, Software, Writing - original draft, Writing - review & editing. **Beatrice Riviere:** Conceptualization, Methodology, Software, Writing - original draft, Writing - review & editing.

References

[1] Lantz R. Rigorous calculation of miscible displacement using immiscible reservoir simulators. Soc Pet Eng J 1970;10(02):192–202.
[2] Todd M, O'Dell P, Hirasaki G. Methods for increased accuracy in numerical reservoir simulator. Soc Pet Eng J 1972;12:515–30.

[3] Todd M, Longstaff W. The development, testing, and application of a numerical simulator for predicting miscible flood performance. J Pet Technol 1972;24(07):874–82.
[4] Killough J, Kossack C. Fifth comparative solution project: evaluation of miscible flood simulators. In: SPE symposium on reservoir simulation. Society of Petroleum Engineers; 1987, p. SPE–16000–MS.
[5] Homsy GM. Viscous fingering in porous media. Annu Rev Fluid Mech 1987;19(1):271–311.
[6] Douglas Jr J, Ewing RE, Wheeler MF. The approximation of the pressure by a mixed method in the simulation of miscible displacement. RAIRO-Anal Numér 1983;17(1):17–33.
[7] Palagi C, Aziz K. Use of Voronoi grid in reservoir simulation. SPE Adv Technol Ser 1994;2:66–77.
[8] Ewing R, Wheeler M. Galerkin methods for miscible displacement problems in porous media. SIAM J Numer Anal 1980;17:351–65.
[9] Ewing R, Russell T. Efficient time-stepping methods for miscible displacement problems in porous media. SIAM J Numer Anal 1982;19:1–67.
[10] Chavent G, Jaffré J. Mathematical models and finite elements for reservoir simulation. Studies in mathematics and its applications, North-Holland; 1986.
[11] Russell T. Time stepping along characteristics with incomplete iteration for a Galerkin approximation of miscible displacement in porous media. SIAM J Numer Anal 1985;22(5):970–1013.
[12] Huang H, Scovazzi G. A high-order, fully coupled, upwind, compact discontinuous Galerkin method for modeling of viscous fingering in compressible porous media. Comput Geosci 2013;263:169–87.
[13] Scovazzi G, Huang H, Collis S, Yin J. A fully-coupled upwind discontinuous Galerkin method for incompressible porous media flows: High-order computations of viscous fingering instabilities in complex geometry. J Comput Phys 2013;252:86–108.
[14] Li J, Riviere B. High order discontinuous Galerkin method for simulating miscible flooding in porous media. Comput Geosci 2015;19(6):1251–68.
[15] Li J, Riviere B. Numerical modeling of miscible viscous fingering instabilities by high-order methods. Transp Porous Media 2016;113:607–28.
[16] Cockburn B, Dong JGB, Restelli M, Sacco R. A hybridizable discontinuous Galerkin method for steady-state convection–diffusion-reaction problems. SIAM J Sci Comput 2009;31(5):3827–46.
[17] Cockburn B, Gopalakrishnan J, Lazarov RD. Unified hybridization of discontinuous Galerkin, mixed, and continuous Galerkin methods for second order elliptic problems. SIAM J Numer Anal 2009;47(2):1319–65.
[18] Cockburn B, Dong B, Guzmán J. A superconvergent LDG-hybridizable Galerkin method for second-order elliptic problems. Math Comp 2008;77(264):1887–916.
[19] Huerta A, Angeloski A, Roca X, Peraire J. Efficiency of high-order elements for continuous and discontinuous Galerkin methods. Internat J Numer Methods Engrg 2013;96(9):529–60.
[20] Samii A, Michoski C, Dawson C. A parallel and adaptive hybridized discontinuous Galerkin method for anisotropic nonhomogeneous diffusion. Comput Methods Appl Mech Engrg 2016;304:118–39.
[21] Cockburn B, Di Pietro DA, Ern A. Bridging the hybrid high-order and hybridizable discontinuous Galerkin methods. ESAIM Math Model Numer Anal 2016;50(3):635–50.
[22] Anderson D, Droniou J. An arbitrary-order scheme on generic meshes for miscible displacements in porous media. SIAM J Sci Comput 2018;40(4):B1020–54.
[23] Dawson C, Sun S, Wheeler MF. Compatible algorithms for coupled flow and transport. Comput Methods Appl Mech Engrg 2004;193(23):2565–80.
[24] Fu G, Qiu W, Zhang W. An analysis of HDG methods for convection-dominated diffusion problems. ESAIM Math Model Numer Anal 2015;49(1):225–56.
[25] Nguyen NC, Peraire J, Cockburn B. An implicit high-order hybridizable discontinuous Galerkin method for linear convection–diffusion equations. J Comput Phys 2009;228(9):3232–54.
[26] Qiu W, Shi K. An HDG method for convection diffusion equation. J Sci Comput 2016;66(1):346–57.
[27] Chen Y, Cockburn B. Analysis of variable-degree HDG methods for convection–diffusion equations. Part II: Semimatching nonconforming meshes. Math Comp 2014;83(285):87–111.
[28] Fabien M, Knepley M, Riviere B. A hybridizable discontinuous Galerkin method for two-phase flow in heterogeneous porous media. Internat J Numer Methods Engrg 2018;116:161–77.
[29] Cockburn B, Gopalakrishnan J. A characterization of hybridized mixed methods for second order elliptic problems. SIAM J Numer Anal 2004;42(1):283–301.
[30] Arnold DN, Brezzi F. Mixed and nonconforming finite element methods: implementation, postprocessing and error estimates. RAIRO-Modél Math Anal Numér 1985;19(1):7–32.
[31] Zhang J, Zhu J, Zhang R, Yang D, Loula AF. A combined discontinuous Galerkin finite element method for miscible displacement problem. J Comput Appl Math 2017;309:44–55.
[32] Dawson C, Russell T, Wheeler M. Some improved error estimates for the modified method of characteristics. SIAM J Numer Anal 1989;26(6):1487–512.
[33] Koval E. A method for predicting the performance of unstable miscible displacement in heterogeneous media. Soc Pet Eng J 1963;3(02):145–54.
[34] Chen H, Li J, Qiu W. Robust a posteriori error estimates for HDG method for convection–diffusion equations. IMA J Numer Anal 2015;36(1):437–62.
[35] Bui-Thanh T. Construction and analysis of HDG methods for linearized shallow water equations. SIAM J Sci Comput 2016;38(6):A3696–719.
[36] Dongarra JJ, Du Croz J, Hammarling S, Hanson RJ. An extended set of FORTRAN basic linear algebra subprograms. ACM Trans Math Softw (TOMS) 1988;14(1):1–17.
[37] Anderson E, Bai Z, Dongarra J, Greenbaum A, McKenney A, Du Croz J, Hammarling S, Demmel J, Bischof C, Sorensen D. Lapack: A portable linear algebra library for high-performance computers. In: Proceedings of the 1990 ACM/IEEE conference on supercomputing. IEEE Computer Society Press; 1990, p. 2–11.
[38] Fabien M, Knepley M, Mills R, Riviere B. Manycore parallel computing for a hybridizable discontinuous Galerkin nested multigrid method. SIAM J Sci Comput 2019;41(2):C73–96.
[39] Fischer P. Parallel multi-level solvers for spectral element methods. In: Proceedings of the third international conference on spectral and high order methods. Houston Journal of Mathematics; 1996, p. 595–604.
[40] Guo X-Z, Katz I. A parallel multi-p method. Comput Math Appl 2000;39(9–10):115–23.
[41] Helenbrook B, Mavriplis D, Atkins H. Analysis of p-multigrid for continuous and discontinuous finite element discretizations. In: 16th AIAA computational fluid dynamics conference. 2003, p. 3989.
[42] Lottes J, Fischer P. Hybrid multigrid/Schwarz algorithms for the spectral element method. J Sci Comput 2005;24(1):45–78.
[43] Toselli A, Widlund O. Domain decomposition methods - algorithms and theory. Springer series in computational mathematics, Springer Berlin Heidelberg; 2006.
[44] Balay S, Abhyankar S, Adams MF, Brown J, Brune P, Buschelman K, Dalcin L, Dener A, Eijkhout V, Gropp WD, Karpeyev D, Kaushik D, Knepley MG, May DA, McInnes LC, Mills RT, Munson T, Rupp K, Sanan P, Smith BF, Zampini S, Zhang H, Zhang H. PETSC users manual. Tech. Rep. ANL-95/11 - Revision 3.11, Argonne National Laboratory; 2019.

[45] Balay S, Gropp WD, McInnes LC, Smith BF. Efficient management of parallelism in object oriented numerical software libraries. In: Arge E, Bruaset AM, Langtangen HP, editors. Modern software tools in scientific computing. Birkhäuser Press; 1997, p. 163–202.
[46] Balay S, Abhyankar S, Adams MF, Brown J, Brune P, Buschelman K, Dalcin L, Dener A, Eijkhout V, Gropp WD, Karpeyev D, Kaushik D, Knepley MG, May DA, McInnes LC, Mills RT, Munson T, Rupp K, Sanan P, Smith BF, Zampini S, Zhang H, Zhang H. PETSc Web page. 2019, URL https://www.mcs.anl.gov/petsc.
[47] Cockburn B, Dubois O, Gopalakrishnan J, Tan S. Multigrid for an HDG method. IMA J Numer Anal 2014;34(4):1386–425.
[48] Li J, Riviere B. Numerical solutions of the incompressible miscible displacement equations in heterogeneous media. Comput Methods Appl Mech Engrg 2015;292:107–21.
[49] SPE comparative solution project model 2. 2017, http://www.spe.org/web/csp/datasets/set02.htm, accessed: 27-05-2017.